PHYSICAL REVIEW B **84**, 180411(R) (2011)

Electronic and magnetic structures of bilayer $La_3Ni_2O_6$ and trilayer $La_4Ni_3O_8$ nickelates from first principles

Soumyajit Sarkar,[1] I. Dasgupta,[2] Martha Greenblatt,[3] and T. Saha-Dasgupta[1,*]
[1]*S.N. Bose National Centre for Basic Sciences, Kolkata 700 098, India*
[2]*Department of Solid State Physics, Indian Association for the Cultivation of Science, Kolkata 700 032, India*
[3]*Department of Chemistry and Chemical Biology, Rutgers University, Piscataway, New Jersey 08854, USA*
(Received 17 August 2011; revised manuscript received 29 October 2011; published 22 November 2011)

We revisit the electronic and magnetic structure of bilayer, $La_3Ni_2O_6$ and trilayer, $La_4Ni_3O_8$ nickelates, in terms of detailed first-principles calculations. Through construction of an axial orbital, we show that the crystal-field splitting obtained in a single layer case, is modified substantially in the multilayer case leading to a near degeneracy of several levels and a possible bistability between low spin and high spin state of Ni in specific cases. The issue needs to be settled by further experimental studies, followed by theoretical investigations.

DOI: 10.1103/PhysRevB.84.180411 PACS number(s): 75.10.Dg, 71.20.Be

Following the success of cuprates in high-T_c superconductivity, attention has been focused on layered materials,[1] such as Ni-based compounds.[2] Ni is next to Cu in the Periodic Table, and if it can be realized in the 1+ oxidation state, may have a similar electronic structure as Cu^{2+}. However, Ni^{1+} oxides are generally found to be chemically unstable. The recent reports[3,4] in synthesizing $La_3Ni_2O_6$ (2-LNO) and $La_4Ni_3O_8$ (3-LNO) with square planar coordination of Ni by O, as in CuO_2, therefore have generated much interest. Both 2-LNO and 3-LNO, containing a bilayer and trilayer of NiO_2 planes, respectively, crystallize in $I4/mmm$ space group, as shown in Fig. 1(a). Both compounds have been investigated experimentally and by first-principles calculations.[4–8] However, issues like the ground-state magnetic structure, the spin state of Ni, the genesis of band structure in terms of hybridization of different degrees of freedom, remain debated.

In this Rapid Communication, we revisit the electronic and magnetic structure of both compounds, in terms of detailed density-functional theory (DFT) study, using the plane-wave based basis as implemented in the VASP code[9] and the muffin-tin orbital (MTO) based linear MTO (LMTO) and Nth-order MTO (NMTO) methods.[10,11] The exchange correlation functional was chosen to be generalized gradient approximation (GGA).[12] The missing correlation beyond GGA at Ni sites was taken into account through GGA+U calculation. For the plane-wave calculations, we used projector augmented wave (PAW) potentials,[13,14] and the wave functions were expanded in the plane-wave basis with a kinetic energy cutoff of 600 eV. Reciprocal-space integrations were carried out with a k mesh of $8 \times 8 \times 6$. The GGA+U calculations were performed with the +U implementation of Dudarev *et al.*[15]

Figure 1(b) shows the basic, non-spin-polarized band structure of 2-LNO and 3-LNO. As is seen, for 2-LNO the conduction band, crossing the Fermi level E_F (set at zero in the figure) and spanning an energy range of about -1 to 2 eV, is dominantly of Ni $d_{x^2-y^2}$ character. The Ni d_{xy}, d_{xz}, d_{yz}, and d_{z^2} dominated bands all lie within an energy range of about -2 to -0.5 eV. The states below ≈ -2 eV are of dominant O-p characters. The large bilayer splitting (bonding-antibonding splitting due to interlayer coupling) between d_{z^2} dominated bands is evident. The k-dependent bilayer splitting among Ni $d_{x^2-y^2}$ dominated bands is also seen, which vanishes at the Γ point and is maximum at the saddle point, as found in cuprates.[16] The basic features of the electronic structure of 3-LNO is similar to that of 2-LNO, barring a few important differences. The interlayer splitting of d_{z^2} dominated bands is larger in the case of 3-LNO, due to the addition of one extra layer, which splits bands into bonding, antibonding, and nonbonding combinations. This results in the d_{z^2} dominated, antibonding band to be pushed closer to Ni $d_{x^2-y^2}$ bands, compared to 2-LNO. The O-p dominant bands, on the other hand, are pushed down compared to the bilayer.

In the next step, we introduced spin polarization and studied four different magnetic structures of Ni spins in a $\sqrt{2} \times \sqrt{2} \times 1$ supercell, (i) ferromagnetic (FM), (ii) A-type antiferromagnetic (AFM) which involves parallel (antiparallel) alignments within (between) the layers (AFM-A), (iii) C-type AFM, which involves antiparallel (parallel) alignments within (between) the layers (AFM-C), and (iv) G-type AFM, which involves antiparallel alignments in all directions (AFM-G). The calculated magnetic moments and the relative energetics of various magnetic configurations, as obtained in plane-wave basis within GGA+U for a choice of $U = 6$ eV and $J = 1$ eV are summarized in Table I. The results do not depend on the choices of U and J values significantly. The double counting correction used for the calculations is that of fully localized limit (FLL). The spin state of Ni in these compounds has been a matter of discussion.[17,18] Given the absence of apical oxygens in the planar coordination of oxygens surrounding the Ni atom, one would expect Ni to be in low spin (LS) state.[3,4] We carried out the fixed moment calculations with the moment of Ni varied over a range in a FM configuration. In the absence of any appreciable charge disproportionation of Ni atoms, the nominal electron count of Ni in 2-LNO (3-LNO) is $d^{8.5}$ ($d^{8.67}$). This would lead to LS Ni moments of $0.5\mu_B$ $(0.67)\mu_B$ for 2-LNO (3-LNO), the corresponding high spin (HS) moments being $1.5\mu_B$ $(1.33)\mu_B$. From the results, presented in Fig. 2, we find the LS to be more stable, compared to HS state by about 0.2–0.3 eV. The stabilization of LS configuration is in agreement with the results obtained in Refs. 5 and 6, but in disagreement with the findings of Refs. 7 and 8. A recent study[17] pointed to different schemes of double counting correction for this discrepancy. We find that even using the FLL scheme, our calculations for FM spin

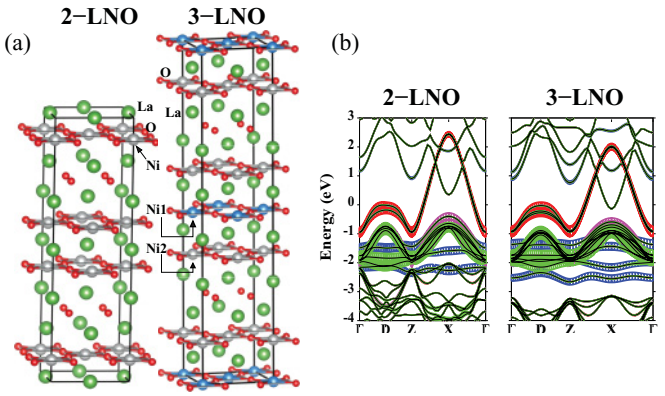

FIG. 1. (Color) (a) Crystal structures of 2-LNO and 3-LNO. (b) Non-spin-polarized band structure of 2-LNO and 3-LNO. The bands are projected onto Ni $d_{x^2-y^2}$ (red), d_{z^2} (blue), d_{xy} (green), and degenerate d_{xz},d_{yz} (magenta) characters.

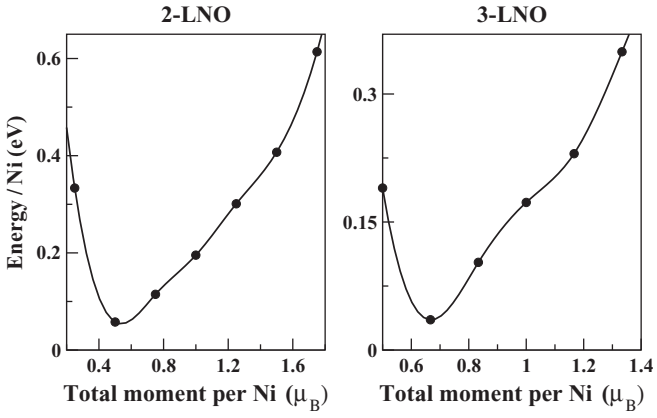

FIG. 2. Total energy plotted as a function of varying magnetic moment for 2-LNO and 3-LNO.

arrangement predict stabilization of the LS state rather the HS state. From Table I, we find that FM and AFM-*A* converge to the LS state with Ni moments close to $0.5\mu_B$ $(0.7)\mu_B$ for 2-LNO (3-LNO). We failed to stabilize the HS states for FM and AFM-*A* configurations. The AFM-*C* and AFM-*G*, on the other hand, were found to either converge to the LS state or the HS state depending on the starting configurations, indicating a bistability with local minima at LS and HS states. The LS state for AFM-*G* and AFM-*C* is energetically more stable compared to HS, with the exception of AFM-*C* for 3-LNO.

The band structures of 2-LNO and 3-LNO for FM, AFM-*A*, AFM-*C*, AFM-*G* are shown in Figs. 3 and 4, respectively. For FM/AFM-*A*, only the majority spin channel is shown, as the states are either filled or empty in the other spin channel.

TABLE I. Total moment (per Ni atom), individual Ni moments, and the total energies of various magnetic arrangements of Ni spins (ΔE), measured from the lowest energy state.

		Total mom. (μ_B)	Ni moment (μ_B)	ΔE/Ni (meV)
	FM	0.50	0.63	0
	AFM-*A*	0.0	−0.64/0.64	0.72
2-LNO	AFM-*C* (HS)	0.0	−1.26/1.25	325
	AFM-*C* (LS)	0.0	−0.61/0.61	265
	AFM-*G* (HS)	0.0	−1.29/1.22	325
	AFM-*G* (LS)	0.0	−0.59/0.59	276
	FM	0.67	0.76	0.48
	AFM-*A*	0.22	0.78/−0.78	0
			−0.76/0.76	
	AFM-*C* (HS)	0.0	−1.41/1.41	77
			−1.22/1.22	
3-LNO	AFM-*C* (LS)	0.0	−0.87/0.87	215
			−0.86/0.86	
	AFM-*G* (HS)	0.01	−1.09/1.02	310
			−1.17/1.15	
	AFM-*G* (LS)	0.0	0.75/−0.74	245
			0.75/−0.74	
	SDW	0.04	0.81/−0.77/0.72	96
			−0.81/0.75/−0.72	
			−0.79/0.74/−0.73	

Considering first 2-LNO, for the LS cases, we consistently find the solutions to be metallic with antibonding Ni-$d_{x^2-y^2}$–O-p σ band crossing E_F, similar to the low-energy orbital composition found in the case of cuprates. For HS cases, on the other hand, the low-energy states are of dominant antibonding Ni-d_{xy}–O-p π character. The ground state for HS, AFM-*C* structure turned out to be semiconducting. For the trilayer case, for the LS cases, though the states are of primarily antibonding Ni-$d_{x^2-y^2}$–O-p σ character, we find an admixture of Ni-d_{z^2} too, seen in terms of formation of a central lobe at the Ni site, which should have a node for pure Ni-$d_{x^2-y^2}$ character. For HS cases, the low-energy states for AFM-*G* are of primarily antibonding Ni-d_{xy}–O-p π character, while that of AFM-*C* type is curious with largely admixed Ni-d_{z^2}-Ni-$d_{x^2-y^2}$ states (cf. insets in Figs. 3 and 4).

Further, we carried out NMTO-downfolding calculations, in which, starting from an all orbital calculation, we kept active only the Ni-*d* orbital degrees of freedom and integrated out the rest.[11] Such calculations are expected to give rise to accurate estimates of the positions of various Ni-*d* levels. In the

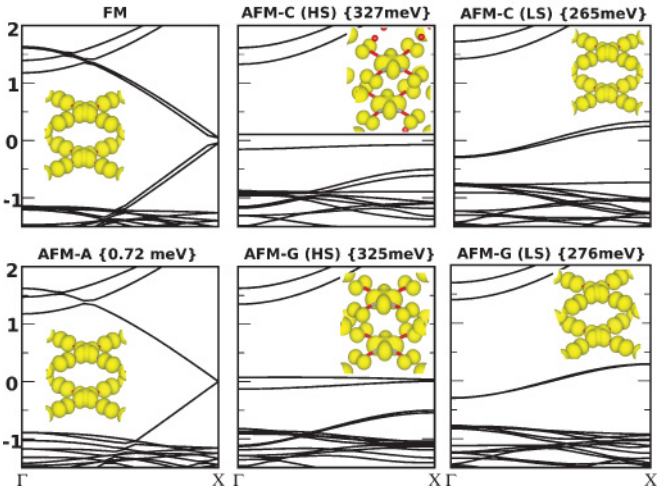

FIG. 3. (Color online) The band structures of 2-LNO. Insets show the charge-density plots corresponding to low-energy bands for each case. The numbers in the brackets in the heading indicate the total energy.

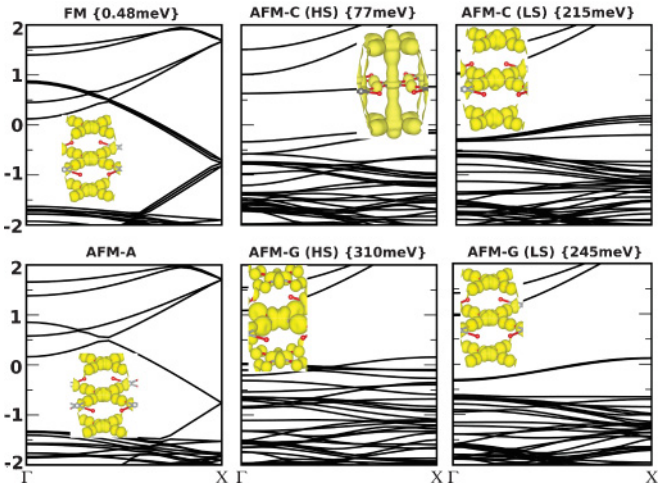

FIG. 4. (Color online) Same as in Fig. 3, but for 3-LNO.

absence of any interlayer coupling, the crystal-field splitting of Ni-d levels at individual NiO_2 layers are shown in the extreme left-hand or right-hand sides in each panel of Fig. 5. For both compounds, we find that planar NiO_2 geometry leads to d_{z^2} level to be the lowest energy, followed by degenerate d_{xz},d_{yz}, and d_{xy} levels in increasing order of energy. The $d_{x^2-y^2}$ level is separated from the rest by a separation of about 1.3–1.4 eV. This level diagram is similar to that in the text book[19] for a square planar geometry and different from that presented in the recent Refs. 7 and 8. The interlayer coupling is mediated by formation of an axial orbital, which is found to be a combination of Ni-s, Ni-d_{z^2}, and O-p.[20] The interlayer coupling gets further strengthened by coupling with La-5d characters, reflected in the tails of the axial orbital, sitting at La sites intervening different layers, as shown in Fig. 5. The energy of the such a renormalized axial orbital is given by $\epsilon_a = \epsilon_{z^2} + \frac{t_{z^2p}^2}{E_F-\epsilon_p} + (\frac{t_{sp}t_{z^2p}}{E_F-\epsilon_p} + t_{s,z^2})^2/(\epsilon_s - E_F + \frac{t_{sp}^2}{E_F-\epsilon_p})$, where ϵ_{z^2}, ϵ_p, and ϵ_s are bare on-site energies of the Ni-d_{z^2}, O-p, and Ni-s. t_{sp} (t_{z^2p}) indicates hopping between Ni-s (Ni-d_{z^2}) and O-p. The hybridization with La and O-p_z introduces an additional hopping interaction between Ni-s and Ni-d_{z^2}, expressed as t_{s,z^2}.

This mixing with Ni-s as well as O-p and La-d strongly renormalizes the Ni-d_{z^2} level, which splits into bonding and antibonding levels for 2-LNO and into bonding, nonbonding, and antibonding levels for 3-LNO. The resulting interlayer splitting for the renormalized Ni-d_{z^2} level, the axial level, is maximum within all the d levels, with the separation between the lowest bonding level and the highest antibonding level to be about 0.8 (1.4) eV for 2-LNO (3-LNO). The interlayer splitting of $d_{x^2-y^2}$, d_{xz},d_{yz}, d_{xy} are small, of the order of 0.2–0.3 eV, arising due to finite mixing with the axial orbital. This causes the renormalized, antibonding Ni-d_{z^2} level to be pushed significantly higher up, positioning it just below (degenerate with) the d_{xy} levels for 2-LNO (3-LNO), as shown in Fig. 5. For understanding the results presented in Figs. 3 and 4, one further needs to add the bandwidth effect, which crucially depends on the alignments of neighboring Ni spins–FM alignments resulting in larger bandwidths compared to AFM alignments. Considering 2-LNO, the population of

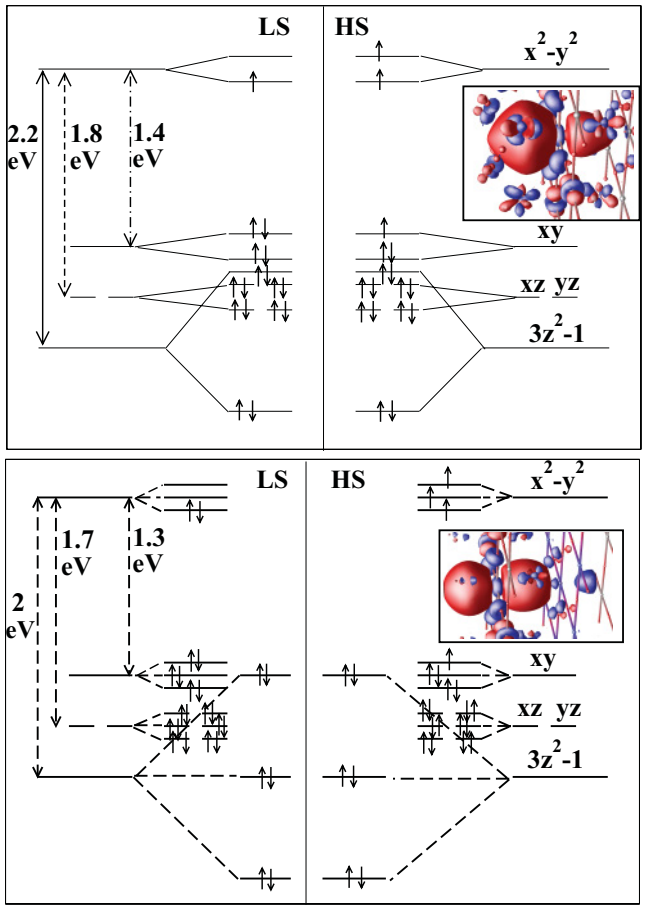

FIG. 5. (Color online) The positions of Ni-d energy levels and their occupancies for LS and HS cases, for 2-LNO (top panels) and 3-LNO (bottom panels). The insets in the right panels show the plot of axial orbitals. Plotted are the constant value surfaces.

levels in the LS situation leads to to the situation that all states except $d_{x^2-y^2}$ are occupied in both spin channels. $d_{x^2-y^2}$ is occupied by one, unpaired electron, causing it to be the low-energy state. This leads to a metallic state due to the large bandwidth of Ni-$d_{x^2-y^2}$–O-p σ bonding and relatively small interlayer splitting of $d_{x^2-y^2}$ states. The population of levels in the HS situation, on the other hand, leads to the situation where all states are occupied in the majority spin channel, and in the minority spin channel bonding d_{xy} state to be the highest occupied state. The small bandwidth offered by Ni-d_{xy}–O-p π bonding in the AFM configuration then may lead to a semiconducting solution with a gap formed between the occupied, bonding d_{xy} state and the unoccupied, antibonding d_{xy} state, as found for the AFM-C case (cf. Fig. 3). For 3-LNO, for the LS cases, the highest occupied state is bonding $d_{x^2-y^2}$ state, giving rise to metallic solutions, while the HS cases are delicate due to near degeneracy between antibonding d_{z^2} and d_{xy} levels. Depending on the bandwidths, which are dictated by the details of the magnetic arrangements, one or the other forms the low-energy band (d_{xy} for AFM-G and d_{z^2} for AFM-C). Also, the band-structure effect causes the $d_{x^2-y^2}$ and renormalized d_{z^2} states to hybridize strongly, which are energetically now separated by about 1 eV compared to $\approx$2 eV for the single layer situation. Finally, for $La_4Ni_3O_8$ an

AFM spin-density-wave (SDW) solution was proposed in Ref. 6 based on the nesting of the Fermi surface. We have also checked the possibility of this solution in our calculation. The calculated total energy per Ni turned out to be 96 meV/Ni (see Table I), placing the AFM-SDW solution in close competition with the AFM-*C* HS solution.

In summary, we have carried out detailed electronic structure calculations of $La_3Ni_2O_6$ and $La_4Ni_3O_8$, which have been discussed in recent literature.[3–8,17,18] Our calculations show that the crystal-field splitting obtained for a single layer planar geometry is modified substantially in the multilayer case causing a near degeneracy of several levels. The interlayer coupling in the multilayer case is assisted by an axial orbital, constructed out of Ni-d_{z^2}-Ni-*s*-O-*p* and interestingly, of La-*d*. Our calculations show, for both compounds, FM- or AFM-*A*-type configurations to be the magnetic ground state (GS), with near degeneracy of the two states. The solutions for FM- or AFM-*A*-type configuration turn out to be metallic. We find the LS states to be energetically more stable for the FM and AFM-*A* configurations. For AFM-*C* and AFM-*G*, we find that convergence is achieved either in the LS state or in the HS state depending on the starting configuration. This leads to bistability, present for the AFM structures of these compounds, and may explain the apparent discrepancies between different DFT results.[6–8,17] For example, the AFM-*C* type was investigated in Ref. 6, however, since the starting configuration was assumed to be that of LS, the convergence only to the LS state was achieved (which is energetically $\approx$200 meV higher than the GS), thereby missing out the energetically comparable state of AFM-*C* (HS) to that of AFM-SDW. The energetics of different magnetic structures were not reported in Ref. 7; the starting configurations were also not discussed. Since both Refs. 6 and 7 used the same basis set and same computer package (WIEN2K) one would expect similar results to be obtained, which, however, may be influenced by the starting configuration, as our study reveals.

At the end, the situation needs to be clarified in terms of further experimental studies. The experiments carried out on polycrystalline samples indicate thermally activated conducting properties, for both compounds, while the minimum-energy states given by DFT are found to be metallic. However, the experimental transport properties may be dominated by poor percolation in the loosely packed powder pellet, or dominated by semiconducting behavior along the perpendicular to layer direction. Unfortunately, so far, the single crystals seem impossible to obtain.[6] For 2-LNO, no magnetic ordering has been found[5] down to 4 K while for 3-LNO, recent neutron diffraction[18] also finds no signature of magnetic reflection at low *T*. Energetics presented in Table I show both AFM-*C* (HS) configuration and SDW to be energetically comparable, and intermediate in energy between AFM-*A*/FM and the high-energy structures like AFM-*G* (LS and HS) or AFM-*C* (LS). It might be possible that either the AFM-*C* (HS) or SDW state is the state obtained experimentally, as a total moment of $0.22\mu_B$ obtained for AFM-*A* (the GS according to present calculation) is not seen experimentally (cf. Fig. S2 in Ref. 6). We need to remember, though, that the AFM-*C* (HS) and SDW state gives rise to two different conducting properties. AFM-*C* (HS) is insulating, while SDW is metallic [cf. density of states (DOS) presented in Ref. 6]. It is worth mentioning at this point that the NMR data, which are a reliable probe for the DOS, show a Korringa term in the low-temperature phase. While the NMR shows a sizable reduction of the DOS at low temperature, it is important to note that the suppression of the DOS is not complete. Therefore to resolve the puzzles, one surely needs a reliable experimental way to extract the charge-transfer gap of the parent compound, which to date is not available.

S.S., I.D., and T.S.D. thank CSIR and DST for financial support, and Badiur Rahaman for initial calculations. M.G. thanks NSF-DMR-0966829 for partial support. The authors acknowledge G. Kotliar and A. Nevidomskyy for discussion.

*tanusri@bose.res.in

[1] Y. Kohama, Y. Kamihara, M. Hirano, H. Kawaji, T. Atake, and H. Hosono, Phys. Rev. B **78**, 020512(R) (2008).

[2] V. I. Anisimov, D. Bukhvalov, and T. M. Rice, Phys. Rev. B **59**, 7901 (1999).

[3] V. Poltavets, K. A. Lokshin, S. Dikmen, M. Croft, T. Egami, and M. Greenblatt, J. Am. Chem. Soc. **128**, 9050 (2006).

[4] V. Poltavets, K. A. Lokshin, M. Croft, T. K. Mandal, T. Egami, and M. Greenblatt, Inorg. Chem. **46**, 10887 (2007).

[5] V. V. Poltavets, M. Greenblatt, G. H. Fecher, and C. Felser, Phys. Rev. Lett. **102**, 046405 (2009).

[6] V. V. Poltavets, K. A. Lokshin, A. H. Nevidomskyy, M. Croft, T. A. Tyson, J. Hadermann, G. Van Tendeloo, T. Egami, G. Kotliar, N. ApRoberts-Warren, A. P. Dioguardi, N. J. Curro, and M. Greenblatt, Phys. Rev. Lett. **104**, 206403 (2010).

[7] V. Pardo and W. E. Pickett, Phys. Rev. Lett. **105**, 266402 (2010).

[8] V. Pardo and W. E. Pickett, Phys. Rev. B **83**, 245128 (2011).

[9] G. Kresse and J. Furthmuller, Phys. Rev. B **54**, 11169 (1996).

[10] O. K. Andersen and O. Jepsen, Phys. Rev. Lett. **53**, 2571 (1984).

[11] O. K. Andersen and T. Saha-Dasgupta, Phys. Rev. B **62**, R16219 (2000).

[12] J. P. Perdew, K. Burke, and M. Ernzerhof, Phys. Rev. Lett. **77**, 3865 (1996).

[13] P. E. Blöchl, Phys. Rev. B **50**, 17953 (1994).

[14] The pseudopotentials used have the following configurations: La: valance electron 11, core configuration [Kr]$4d^{10}$; Ni: valance electron 10, core configuration [Ar]; O: valance electron 6, core configuration $1s^2$.

[15] S. L. Dudarev, G. A. Botton, S. Y. Savrasov, C. J. Humphreys, and A. P. Sutton, Phys. Rev. B **57**, 1505 (1998).

[16] O. K. Andersen, A. I. Liechtenstein, O. Jepsen, and F. Paulsen, J. Phys. Chem. Solids **56**, 1573 (1995).

[17] V. Pardo and W. E. Pickett (unpublished).

[18] T. Egami *et al.*, e-print arXiv:1106.4828.

[19] G. L. Miessler and D. A. Tarr, *Inorganic Chemistry*, 3rd ed. (Prentice-Hall, Englewood Cliffs, NJ, 2003).

[20] E. Pavarini, I. Dasgupta, T. Saha-Dasgupta, O. Jepsen, and O. K. Andersen, Phys. Rev. Lett. **87**, 047003 (2001).